arXiv:1601.04608v2 [cond-mat.stat-mech] 17 Sep 2016

Hallmarks of the Kardar-Parisi-Zhang universality class elicited by scanning probe microscopy

Sidiney G. Alves,[1] Clodoaldo I. L. de Araujo,[2] and Silvio C. Ferreira[2]

[1] *Departamento de Física e Matemática, Universidade Federal de São João Del-Rei, 36420-000, Ouro Branco, Minas Gerais, Brazil*

[2] *Departamento de Física, Universidade Federal de Viçosa, 36570-000, Viçosa, Minas Gerais, Brazil*

Scanning probe microscopy is a fundamental technique for the analysis of surfaces. In the present work, the interface statistics of surfaces scanned with a probe tip is analyzed for both *in silico* and experimental systems that, in principle, *do not* belong to the prominent Kardar-Parisi-Zhang (KPZ) universality class. We observe that some features such as height, local roughness and extremal height distributions of scanned surfaces quantitatively agree with the KPZ class with good accuracy. The underlying mechanism behind this artifactual KPZ class is the finite size of the probe tip, which does not permit a full resolution of neither deep valleys nor sloping borders of plateaus. The net result is a scanned profile laterally thicker and higher than the original one implying an excess growth, a major characteristic of the KPZ universality class. Our results are of relevance whenever either the normal or lateral characteristic lengths of the surface are comparable with those of the probe tip. Thus our finds can be relevant, for example, in experiments where sufficiently long growth times cannot be achieved or in mounded surfaces with high aspect ratio.

I. INTRODUCTION

Universality beyond scale invariance and critical exponents is well established in both equilibrium [1, 2] and nonequilibrium [3] critical systems. Universal fluctuations underlying the interface growth were sown by Krug *et al.* [4] in the framework of the Kardar-Parisi-Zhang (KPZ) universality class [5], represented by the nonlinear stochastic equation governing the surface height evolution $h(\mathbf{x},t)$

$$\frac{\partial h}{\partial t} = \nu\nabla^2 h + \frac{\lambda}{2}|\nabla h|^2 + \eta. \tag{1}$$

The first and third terms in the right-hand side of Eq. (1) represent, respectively, the surface tension and a white noise given by $\langle\eta\rangle = 0$ and $\langle\eta(\mathbf{x},t)\eta(\mathbf{x}',t')\rangle = 2D\delta(\mathbf{x}-\mathbf{x}')\delta(t-t')$. The second term represents a fundamental benchmark of the KPZ class [5]: the surface grows locally faster (or slower if $\lambda<0$) than the rate of particles arriving at the surface, resulting in an *excess velocity*. The KPZ equation is a fundamental example that follows the Family-Vicsek scaling [6], in which the variance of the height profile (also called squared interface width or roughness) obeys the ansatz $w^2(l,t) = t^{2\beta} f(l/t^{\beta/\alpha})$ as a function of time t and scale of measurement l. The function $f(x)$ scales as $f(x) \sim x^{2\alpha}$ for $x \ll 1$ and $f(x) \sim$ const if $x \gg 1$. The growth (β) and roughness (α) exponents yield the interface scaling in the transient and stationary regimes as $w \sim t^{\beta}$ and $w \sim l^{\alpha}$ for $t \ll l^{\alpha/\beta}$ and $t \gg l^{\alpha/\beta}$, respectively [7].

Consider a d_s+1-dimensional system where d_s is the dimension of the growth substrate. Krug *et al.* [4] proposed that a flat initial condition in 1+1-dimensional KPZ surfaces asymptotically leads to the ansatz

$$h = v_\infty t + \mathrm{sgn}(\lambda)(\Gamma t)^{\beta}\chi, \tag{2}$$

where v_∞ is the asymptotic growth velocity, Γ is a parameter associated to the amplitude of the interface width, $\beta = 1/3$ is the growth exponent in $d = 1+1$, and χ is a universal stochastic quantity whose distribution does not depend on the microscopic details of the model but does on the boundary and initial conditions [8]. It is worth to remark that analytical [9, 10] and experimental [11] confirmations of the KPZ ansatz were obtained first in curved geometry. Posteriorly, this conjecture was confirmed in several independent works [12–14]. The distribution of χ is known in $d = 1+1$ for a flat initial condition [12] as the Tracy-Widom distribution of the largest eigenvalue of the Gaussian orthogonal ensemble (GOE) [15].

Despite of the lack of rigorous results in $d = 2+1$, a meticulous analysis of several models [16–18], accepted as belonging to the KPZ class, and the numerical integration of the KPZ equation itself [16] strongly indicate that the ansatz given by Eq. (2) also holds for the three-dimensional case with the corresponding growth exponent $\beta = 0.241$ and a new universal stochastic quantity χ with mean $\langle\chi\rangle \simeq -0.83$, variance $\langle\chi^2\rangle_c \simeq 0.237$, skewness $S = \langle\chi^3\rangle_c/\langle\chi^2\rangle_c^{1.5} \simeq 0.43$, and kurtosis $K = \langle\chi^4\rangle_c/\langle\chi^2\rangle_c^2 \simeq 0.35$ [16, 17, 19]. Hereafter, $\langle X^n\rangle_c$ is the nth cumulant of X. Very recently, an analogous of the KPZ ansatz for a universality class different from KPZ has been proposed [20].

Earlier attempts of experimental realizations of the 2+1-KPZ class through scaling exponents were not fully conclusive due to experimental limitations as, for example, short times and length scales as well as instabilities caused by interlayer diffusion barriers [21] (See also Refs. [22–24] for more examples and references) and only a few experiments reporting scaling exponents consistent with the 2+1-KPZ class are known [25, 26]. In particular, the deposition of organic films on silicon substrates [25] provided $\beta = 0.28(4)$ and $\alpha = 0.45(5)$ (using approximately 1 decade in power law regressions), which are consistent, within uncertainties, with the accepted 2+1-KPZ exponents $\beta \approx 0.24$ and $\alpha \approx 0.39$ [27]. The results

of Ref. [25] were recently revisited [28] and height distributions shifted to null mean and unitary variance are fitted by the distributions of the $2+1$-KPZ class within four orders of magnitude. Also, preceding the studies of [28], rescaled KPZ height distributions were found in the growth of CdTe semiconductor films [29, 30]. The experimental realization of the $2+1$-KPZ class was further supported in [28–30] by the agreement between local roughness [31] and extremal height [32, 33] distributions with the corresponding $2+1$-KPZ curves. Furthermore, spatial correlators in good agreement with 2+1-KPZ class were also presented [28]. Even in cases where the scaling exponents deviate considerably from the KPZ ones, rescaled distributions have been pointed as robust and little sensitive to finite time and size effects [30].

A common feature in Refs. [25, 28–30] is that the analyzed surfaces were acquired through atomic force microscopic (AFM) technique. However, the nonlinear smoothing effects caused by the finite size of the probe tip can introduce subtle but relevant biases in the experimental determination of scaling exponents of self-affine surfaces [34, 35]. Motivated by the experimental observations of KPZ distributions and the well known smoothing effect inherent to the scanning probe microscopy (SPM) technique [34], we investigated the role played by a probe tip in the statistics of surfaces. We analyzed computer models and the electrodeposition of iron on silicon substrates, systems that do not belong to the KPZ universality class. We observe that the scaled KPZ distributions can be found in the scanned surfaces when the original ones *do not belong* to the KPZ class. The growth exponents become closer to the KPZ value for scanned than for original interfaces. Also, the average growth velocity of the scanned surface is apparently consistent with the KPZ ansatz. We observed the aforementioned accordance when the scanning probing tip scales are comparable with the characteristic lengths of the surface and introduce a non-negligible excess of height in the profiles.

The paper layout is organized as follows. In section II, we discuss the effects of a scanning probe tip on the statistics of growing surfaces using models which are known as not belonging to the KPZ class. In section III, we analyze the electrodeposition of iron on silicon substrates as an experimental example of KPZ distributions produced by tip effects. In section IV, some strategies to rule out false positives for KPZ are discussed and in section V we summarize our conclusions and draw some prospects.

II. SPM SURFACES AND THE KPZ CLASS

The rationale for a potential false positive of KPZ class is pictorially shown in the upper insertion of Fig. 1(c) where the scanning of an originally rough surface brings forth a smoothed profile; See also Figs. 1 and 2 in Ref. [34]. Here, more important than the short wavelength smoothing, which affects the determination of the roughness exponent [34], is that the profiles are laterally thicker having a local height higher than the original one and it represents a central mechanisms behind the KPZ equation: normal growth and excess velocity [5, 7]. Might this artifact introduce traits of the KPZ class? To shed light in this issue we analyzed surfaces numerically obtained with a simple irreversible model for molecular beam epitaxy (MBE), in which each deposited particle starts to diffuse randomly with probability p^{n+1}, where n is the number of bonds in the same deposition layer, or gets irreversibly stuck with the complementary probability. A step barrier [21] for diffusion is also included as a probability P_D to diffuse downwardly leading to mounded instead of self-affine surfaces, as shown in Fig. 1(a). We present results for $p = P_D = 0.9$. We also analyzed the classic Wolf-Villain (WV) [36] and Das Sarma-Tamborenea (DT) [37] models (see also [7] for model definitions), which are known as not belonging to the KPZ class. In $d = 2+1$ dimensions, these models have upward currents induced by the configurations of the neighborhood of particles deposited on steps and asymptotically produce mounded surfaces [38]. All simulations were done on square lattices with periodic boundary conditions.

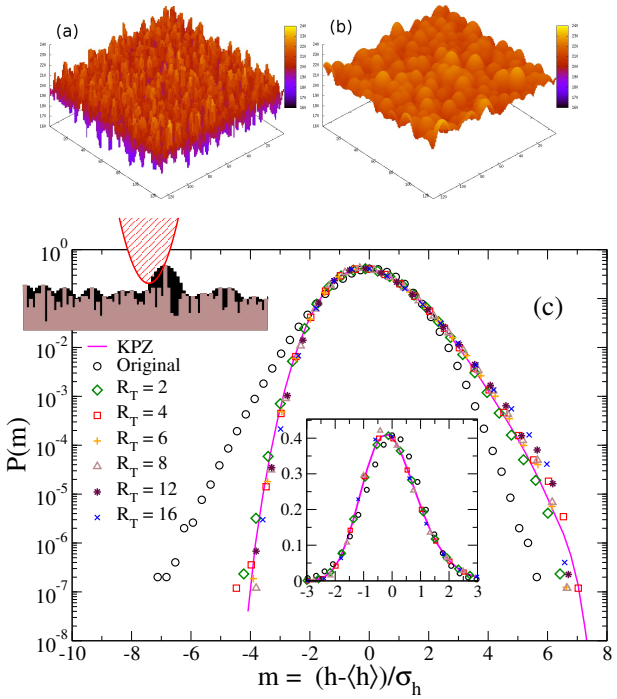

FIG. 1. Original (a) and scanned (b) surfaces generated with the $2+1$-MBE model. (c) Height distributions rescaled to mean zero and variance 1 for parabolic tips of different sizes. The system size is 2048×2048 and the growth time $t = 250$. A $2+1$-KPZ (RSOS model) distribution is also shown. Inset: the same distributions in linear scales. Upper insertion illustrates the effect of the scanning probe tip.

We constructed the scanned surface $\tilde{h}(\mathbf{x})$ following Lechenault *et al.* [34]: $\tilde{h}(\mathbf{x}) = \max_{\mathbf{x}'}[h(\mathbf{x}') - g_R(\mathbf{x}-\mathbf{x}')]$, where g_R gives the shape of the tip and R_T its radius

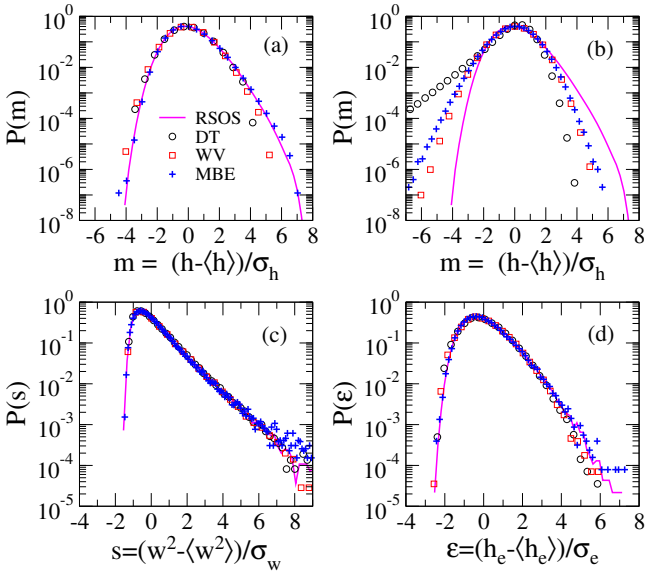

FIG. 2. (Color online) (a) Height, (c) local roughness, and (d) extremal height probability distributions scaled to mean 0 and variance 1 for scanned surfaces of distinct models. The height distributions for original surfaces are shown in panel (b). The solid curves correspond to the KPZ surface in all panels. A parabolic tip of radius $R_T = 16$ was used in DT and WV and $R_T = 4$ for MBE surfaces. Other tip sizes were checked and the results did not change. For all models, 120 monolayers were deposited on 2048×2048 square lattices.

.

of curvature. We present the results for a parabolic shape $g_R = |\mathbf{x}|^\gamma/2R_T^{\gamma-1}$, with $\gamma = 2$ frequently found in real tips [34]. We checked different tips (square that corresponds to $\gamma \gg 1$, semi-circle and other values of $\gamma > 2$) and the central conclusions were independent of the shape.

Experimental surfaces analyzed with SPM are two-dimensional. So, we will present the results for $d = 2+1$ remarking that similar conclusions hold for $d = 1+1$. The effect depicted in the top insertion of Fig. 1(c) is enhanced in $d = 2+1$ since both longitudinal and transversal directions contribute to the growth excess. Original and scanned surfaces for the MBE model are compared in Figs. 1(a) and (b). Specification of high quality commercial AFM tips provides $R_T \lesssim 10$ nm. Assuming a typical lattice constant of semiconductor materials as 0.5 nm, the tip sizes used in Fig. 1 are at least as sharp as the best commercial tips. It is worth to note that a tip radius specification refers only to the sharpest part of the setup while its bulk, that can also interact with the surface depending on the involved lengths, is much larger. The height distributions shifted to mean zero and scaled to variance 1, $m = (h - \langle h \rangle)/\sigma_h$ where $\sigma_h = \sqrt{\langle h^2 \rangle_c}$, are shown in Fig. 1(c) for the MBE model. This approach is widely used to evaluate the universality of distributions in numerics and experiments (e.g. [25, 28–31, 39] and references therein). The height distributions for the original surfaces deviate from the KPZ one, which is here represented by the restricted solid-on-solid (RSOS) model [40, 41], in both tails and peak. However, for tips of sizes in the range $R_T = 2$ to 8, the distributions of the scanned surfaces are remarkably close to the KPZ one. For $R_T \gtrsim 10$ the tip is larger than the typical mound radius ($\xi \approx 5$), the scanned surfaces become smoother and the right tail starts to deviate from the KPZ curve, but it is still consistent with KPZ at least up to 10^{-4}. Analogous results were obtained for WV and DT models, as illustrated in Figs. 2(a) and (b), with a difference that larger tips provide the better accordance with KPZ. In case of WV and DT surfaces, we observed the agreement with KPZ distributions in a narrower range of tip sizes where R_T is close to ξ. However, in a mounded structure with high aspect ratio (height/width), the bulk of the tip can contribute to increase the lateral width of the scanned profile. In MBE model, for example, the original surfaces present mounds of high aspect ratio and the KPZ distribution is still observed for a relatively tiny tip of diameter $R_T = 2$ which is considerably smaller than the typical mound radius of about $\xi \approx 5$.

Skewness and kurtosis are highly dependent on the tails and, therefore, are key parameters to determine the universality of the distributions. Experimentally, it is very hard to obtain accurate estimates of them due to the limited resolution in the tails of the height distributions. To the best of our knowledge, experimental systems providing estimates of both skewness and kurtosis in clear agreement with KPZ are restricted to $d = 1+1$ [11, 14, 42] and used video microscopy to acquire the interfaces being, therefore, rid of the mechanism investigated in the present work. For SPM analyses, positive skewness [28] or estimates with large uncertainties [29, 30] were reported. For a fixed growth time, we observed that both skewness and kurtosis increase with the tip size, since the lowest height contributions are being depleted, but values consistent with KPZ ($S = 0.4$ to 0.5 against 0.43 and $K = 0.3$ to 0.5 against 0.35) are observed for R_T comparable to ξ; See also discussion on Fig. 3 for time dependence. A related result was obtained in Ref. [43], where the profile statistics of equipotentials, which are akin to the output profile in SPM techniques, generated by self-affine conducting surfaces yield a large skewness for a growth model in the regime of the linear Edwards-Wilkinson universality class [7], for which $S = 0$.

Recently, roughness [31, 44] and extremal height [32, 33, 44, 45] distributions inside boxes of size $1 \ll \ell \ll L$ with open boundary conditions have been used as signatures of the KPZ class in experiments [28–30, 46]. In Figs. 2(c) and (d), these (scaled) distributions are compared with the KPZ ones, where boxes of size $\ell = 16$ were used. No significant difference in the distributions was observed in the range $\ell = 8$, 16 and 32 where we measured 2.03, 1.97, and 2.08, respectively, for the skewness of the local roughness distribution of the MBE model at time $t = 120$. This values are in agreement with previous reports [28, 29]. The distributions for the original surfaces are not very different from the KPZ one (data

not shown) as pointed recently in simulations of models in the Villain-Lai-Das Sarmas universality class [47], but in our simulations the distributions for scanned surfaces are indistinguishable from KPZ. It is worth noticing that these distributions vary less with the tip size than the height distribution.

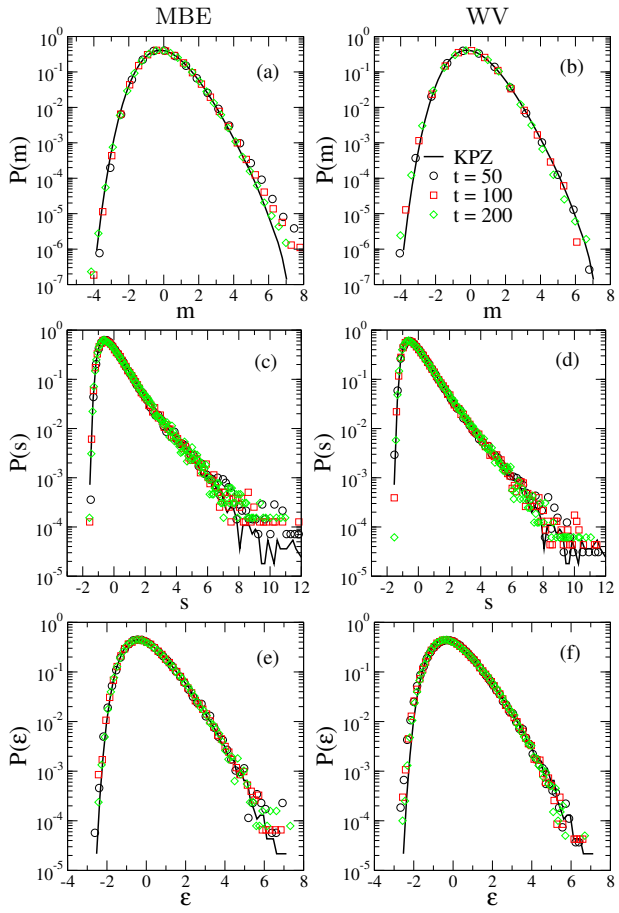

FIG. 3. (Color online) Scaled distributions at different times for MBE (left) and WV (right) models in $d = 2 + 1$ dimensions. The height distributions were rescaled to mean zero and variance 1. Height (top), squared roughness (middle), and extremal height (bottom) distributions are shown. The system size is $L = 2048$ and the tip sizes are $R_T = 4$ and $R_T = 8$ for MBE and WV models, respectively. The KPZ distributions (RSOS) are also shown.

The comparison of the distributions of scanned surfaces at different times with KPZ can be seen in Fig. 3, showing that the results are visually robust withing this time window. One interesting feature observed for MBE is that the skewness initially approaches the KPZ value $S_{\rm KPZ} = 0.43$ as time increases in analogy with the finite-time corrections observed in experiments [11, 14, 48] and simulations [13, 17, 39, 49] of actual KPZ systems. For example, the skewness of the height distributions in MBE are $S = 0.55,\ 0.49,\ 0.45$, and 0.41 for $t = 50,\ 100,\ 200$ and 500 but, differently from actual KPZ systems, it keeps decreasing and start to deviate considerably from

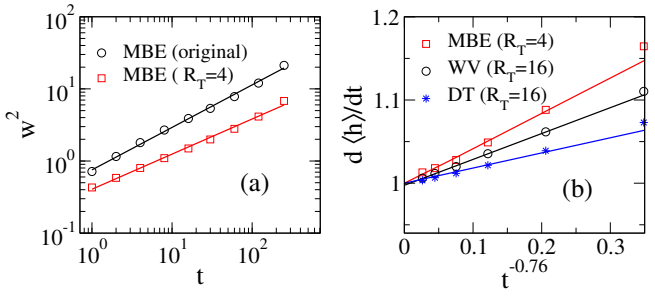

FIG. 4. (Color online) (a) Squared interface width against time for scanned and original surfaces of $2 + 1$-MBE model. (b) Interface velocity against $t^{-1+\beta_{kpz}}$ for three models. The solid lines are linear regressions.

KPZ for longer times. Actually, we expect that it must converge to $S_{MBE} = 0$ for very long times due to mounds increasing approximately independently [50] are expected to render a normal distribution. For WV and DT the values move away since shorter times and must converge to lower values $S \approx 0$ because WV and DT models asymptotically exhibit mounded morphology in $d = 2 + 1$ [38]. Thus, the KPZ trait produced by the finite-size tip is a transient behavior which is relevant when the surface characteristic lengths are comparable with the tip size. However, for the MBE model, the aspect ratio of the mounds initially increases with time, producing deeper valleys and increasing the excess growth introduced by the tip convolution and thus the KPZ hallmarks are enhanced as time evolves. Note that the origin of the mounded morphology is the step barrier to downhill diffusion [21, 51] and its existence has been proposed in many experiments involving thin film growth of metals, semiconductors [21] and organic materials [52, 53].

We also analyzed the kinetic roughening during a short time interval (≈ 2 decades), collecting data for 10 different times and 10 independent samples for each time, mimicking conditions reproducible in experiments. Interface width for scanned surfaces has a quite satisfactory scaling in time, Fig. 4(a), with growth exponents $\beta = 0.24$ (0.30), 0.25 (0.23), and 0.25 (0.24) for MBE, WV and DT models, respectively. The numbers in parenthesis are the exponents for the original surfaces. Notice that in DT and WV models, the exponents for the original surfaces at short times are expected to be given by the linear Mullins-Herring equation [7] with $\beta = 0.25$ and are, inside the numerical accuracy, indistinguishable from the KPZ exponent $\beta \approx 0.24$. However, for the original surfaces of MBE model the growth exponent is different from the KPZ one at short time while the scanned surfaces exhibit a growth exponent consistent with KPZ. A growth exponent closer to KPZ in scanned than in the original surfaces ar short times is a behavior observed in other simulations we did. For example, for the Family model [54] in $d = 1 + 1$, which has an exponent $\beta \approx 0.25$, we found $\beta = 0.29$ in the scanned surface that approached to the one-dimensional KPZ exponent

$\beta = 1/3$.

According to the KPZ ansatz, Eq. (2), the surface growth velocity is given by

$$\frac{d\langle h\rangle}{dt} = v_\infty + \mathrm{sgn}(\lambda)\beta\Gamma^\beta\langle\chi\rangle t^{\beta-1}, \qquad (3)$$

such that plotting the interface velocity against $t^{\beta-1}$ must provide a linear extrapolation to v_∞ if the KPZ growth exponent is used. Such behavior is confirmed in Fig. 4(b) for all analyzed models, which extrapolate to $v_\infty = 1$. This result is not expected for conservative dynamics, as in the models investigated here, where $v \equiv$ const independently of time.

III. ELECTRODEPOSITION EXPERIMENTS

We also investigated an experimental counterpart of this problem using electrodeposition of iron on silicon substrates. Electrodeposition is a electro-convective, diffusive and, therefore, nonlocal process [55] and is not expected to belong to the KPZ class. Indeed, electrodeposition of cooper [56] and iron [57] thick films revealed anomalous (non self-affine) scaling. Profiles were acquired using AFM under both contact and tap modes and using scanning electron microscopy (SEM), the last one rendering surfaces rid of tip effects. We used PPP-NCSTR Nanosensors^{TM} tips with nominal radius of less than 10 nm and height of 10-15 μm.

The iron films were grown on lightly-doped 1kΩ·cm, n-type (100) silicon substrate in an area of about 0.5 cm^2 after native oxide cleaning by Hidrofluoric acid. Preparation of the bath solution for the electrodeposition, (containing 0.5 M Fe_2SO_4 and 0.5 M $NaSO_4$), followed the protocol described in the literature [58] with controlled pH = 2.5 and using a potentiostatic mode under a potential of -1.8 V. AFM and SEM images of 4×4 μm^2 with a resolution of 1024×1024 pixels were acquired. The SEM images were processed with a standard blur (low-pass) filter to erase the effects of electric accumulation in the grain borders. The gray-scale of SEM images was linearly converted to a height interval $0 \leq \tilde{h} \leq 1$ [59]. Even though the vertical resolution cannot be obtained with SEM, the gray-scale method has been used to estimate fractal dimensions in semiconductor surfaces [59]. For our purpose, the actual height scale does not matter since distribution is shifted to zero mean and variance 1. Possibly the linear assumption in gray-scale method is a rough approximation but it is enough to show that the surface distribution is inconsistent with KPZ.

Figures 5(a) and (b) show a film surface for $t = 150$s generated by AFM (contact mode) and SEM, respectively. Five samples were used for statistics. The SEM image reveals a surface with large grains ($\sim$300 nm) where the substrate still can be resolved, in contrast with smoothed surface produced by the AFM technique. The film approximate thickness is $\sim$ 500 nm implying in a high aspect ratio. The rescaled height distributions are compared with the KPZ one in Fig. 5(c), in which one can see that the SEM provides a bimodal distribution whereas the smoothed AFM surfaces are very close to the KPZ distribution. The bimodal distribution reflects the co-existence of small and large grains, the former having lower growth rates due to the screening effects caused by the latter. Local roughness [Fig. 5(d)] and extremal height (data not shown) distributions of the AFM images are not distinguishable from the KPZ curves whereas those for SEM are. Here we have an example where the tip effect is relevant even when the typical lateral length is much larger than the tip specification. No significant difference between contact and tap modes was observed.

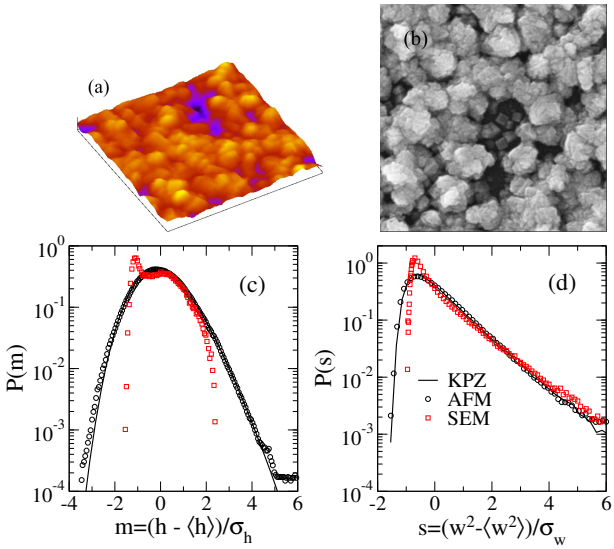

FIG. 5. (Color online) 4×4 μm^2 images of iron films after a growth time $t = 150$ s obtained with (a) AFM in contact mode and (b) SEM imaging techniques. (c) Height and (d) local roughness distributions scaled to mean zero and variance 1 obtained with AFM and SEM are compared with the KPZ class.

IV. RULING OUT FALSE POSITIVES

Summed up the observations reported in the previous section, it is worth to point out strategies to rid the analysis from this tip induced KPZ traits. There exist other KPZ hallmarks that could be used to confirm the universality as, for example, temporal and spatial correlation functions (see, e.g., [28, 48, 60, 61] and references therein). The former requires a huge amount of data for a reliable analysis and therefore are not currently feasible in experiments with SPM. For the latter, a good agreement between experimental data for organic films and 2 + 1-KPZ models was reported [28]. The spatial covariance is given by

$$C_s(r) = \langle h(\mathbf{x}+\mathbf{r})h(\mathbf{x})\rangle - \langle h^2\rangle \simeq (\Gamma t)^{2\beta} G\left[\frac{A_h r^{2\alpha}}{2(\Gamma t)^{2\beta}}\right] \quad (4)$$

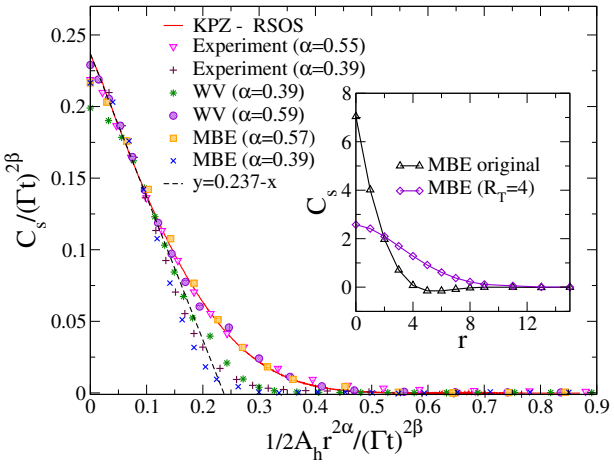

FIG. 6. (Color online) Scaled spatial covariance for MBE and WV surfaces scanned with probe tips of sizes $R_T = 4$ and $R_T = 16$, respectively, are shown. Two values of α were used: theoretically conjectured for KPZ and directly measured by the best data collapse. The covariance for the KPZ class is also shown. Inset shows the original and scanned surfaces for MBE model without rescaling showing the mounded surface signature (minimum in C_s) for the former but not for the latter. The error bars are slightly larger (experiments) or smaller (simulations) than symbols and were omitted for sake of clearness.

where the brackets represent average over positions and samples, $G(x)$ is a scaling function and A_h a phenomenological parameter to be determined. The parameter A_h of the spatial correlators could, in principle, be determined using the Krug-Meakin method [62]. However, we follow the recipe of Ref. [28], suited to experimental data: we plot $G(u) = C_s/(\Gamma t)^{2\beta}$ against $u = \frac{1}{2}A_h r^{2\alpha}/(\Gamma t)^{2\beta}$ and fit Γ and A_h to provide $G(0) = \langle\chi^2\rangle_c = 0.237$ with a slope -1 for $u \approx 0$. For $r \ll R_T$ the surface is essentially smooth and, therefore, we excluded $r < R_T/2$ from the fit procedure. The parameters were therefore extracted fitting the data in range $R_T/2 < r < R_T$ to extrapolate to $\langle\chi^2\rangle_c$ with a slope -1 at $u = 0$. If the rescaling is performed with the accepted KPZ exponent $\alpha = 0.39$ [27], the estimates for scanned surfaces are $A_h \approx 0.94$ and $(\Gamma t)^{2\beta} \approx 11.9$ for MBE and $A_h \approx 0.32$ and $(\Gamma t)^{2\beta} \approx 5$ for WV models. For the electrodeposition experiments, the values are $A_h \approx 90$ and $(\Gamma t)^{2\beta} \approx 1210$.

Figure 6 compares the scaled spatial covariance of MBE and WV models and electrodeposition films with the $2+1$-KPZ curve. The obtained correlation functions clearly deviate from the curve expected for the KPZ class if the accepted KPZ exponent [27] $\alpha = 0.39$ is used, indicating that this analysis succeeded the test and does not provide a false positive. We could also simultaneously fit α looking for the best collapse. In this case, exponents larger than the KPZ one ($\alpha = 0.57$, $\alpha = 0.59$, 0.55 for MBE, WV, and experiments respectively) are obtained pointing out again that the system is not KPZ. Notice, however, that a very nice collapse with the KPZ curve is found when the non-KPZ α exponents are used, Fig. 6, configuring a potential false positive.

Even though the growth exponent β approaches the KPZ class after scanning and could potentially induce a false positive, in many situations the value can still be far from KPZ, as aforementioned for Family model [54] in $d = 1 + 1$. So, the roughness and growth exponents, in the canonical way [7], are the basic starting points for the verification of the KPZ class. Other measurements such as distributions and correlators are fundamental to complement the analysis.

Other possible path is to analyze the actual distribution of χ without the scaling to mean 0 and variance 1, *i. e.*, as performed in the experimental realization of $1+1$-KPZ class [11, 14]. For example, curved and flat KPZ subclasses are, in practice, indistinguishable if this null mean and unity variance strategy is used; See Fig. 6 of Ref. [63], for example. Alternatively, one could fix either average or variance to unity (not to zero) extracting all remaining KPZ properties [17, 49]. The slope of plots $d\langle h\rangle/dt$ versus $t^{\beta-1}$ yields $g_1 = \mathrm{sgn}(\lambda)\beta\Gamma^\beta\langle\chi\rangle$ whereas $g_2 = \langle h^2\rangle_c/t^{2\beta}$ yields $\Gamma^{2\beta}\langle\chi^2\rangle_c$ such that the ratio $R = \beta^2 g_2/g_1 = \langle\chi^2\rangle_c/\langle\chi\rangle^2 \approx 0.32$ is a universal KPZ value [17]. We obtained $R \approx 0.13$, 0.09 and 0.15 for MBE, WV and DT models, which are not consistent with the $2+1$-KPZ class. Note that the scanned surfaces have a positively skewed height distributions that implies $\lambda > 0$. However, at the light of the KPZ ansatz, the positive slope Fig. 4(b) implies that $\langle\chi\rangle > 0$ contrasting with negative $2+1$-KPZ value of -0.83 [16, 41].

V. CONCLUSIONS

In summary, we provide evidences that SPM can artificially introduce traits of the KPZ class in systems where they are not expected. The false KPZ hallmarks were observed in models when the tip convolution introduces a non-negligible excess growth in the original surface. This situation was more clearly observed when the tip specification radius was comparable with the characteristic correlation lengths of rough surfaces or when the surfaces have mounds with a high aspect ratio (height/width) due to the interaction with the tip bulk. Experimental results for electrodeposition of iron also support that KPZ traits are enhance by high aspect ratios. The underlying mechanism of the KPZ features is the excess velocity introduced by the probe tip scanning. While, on the one hand, it was recently shown that the surface smoothing facilitate the unveiling of the universality in genuine KPZ systems with strong correction to the scaling [64, 65], on the other hand, it can introduce artificial traits in dynamics different from KPZ. We also discussed ways to rule out false positives for KPZ. It is important to remark that we observed artificial KPZ traits only for relatively short times and as $t \to \infty$ the characteristic lengths become much larger than the tip size and the excess growth introduced by the scanning must become negligible. However,

it is possible to figure out situations where the artificial KPZ properties can last for long times.

A possible explanation for experimental observations of the KPZ class using SPM was given. Experimental realization of the KPZ class with SPM must assure that the tip probe effects are negligible. Concerning some of the experimental realizations of the KPZ class in 2+1 dimensions [18, 25, 29, 30], the AFM images shows that typical characteristic lengths extracted from correlation functions are considerably above a typical tip radius of 10-20 nm. However, a high aspect ratio cannot be discarded using only AFM images since the deeply grooved regions cannot be resolved with this technique. A systematic analysis of tip size or using non-contact scanning methods such as SEM in these experimental systems would be interesting future works.

ACKNOWLEDGEMENTS

This work was partially supported by the Brazilian agencies CNPq and FAPEMIG. We thank Maxmiliano Munford, Renan Almeida, and Thiago de Assis for motivating discussions. We also thank Rodolfo Cuerno, Tiago Oliveira and Sukarno Ferreira by their critical opinions on the manuscript.

[1] V. Privman, ed., *Finite Size Scaling and Numerical Simulation of Statistical Systems* (World Scientific, Singapore, 1990).

[2] K. Binder, "Finite size scaling analysis of Ising model block distribution functions," Z. Physik B - Condensed Matter **43**, 119 (1981).

[3] M. Henkel, H. Hinrichsen, S. Lübeck, and M. Pleimling, *Non-equilibrium phase transitions*, Vol. 1 (Springer, Berlin, 2008).

[4] J. Krug, P. Meakin, and T. Halpin-Healy, "Amplitude universality for driven interfaces and directed polymers in random media," Phys. Rev. A **45**, 638 (1992).

[5] M. Kardar, G. Parisi, and Y.-C. Zhang, "Dynamic scaling of growing interfaces," Phys. Rev. Lett. **56**, 889 (1986).

[6] F. Family and T. Vicsek, "Scaling of the active zone in the Eden process on percolation networks and the ballistic deposition model," J. Phys. A: Math. Gen. **18**, L75 (1985).

[7] A.-L. Barabasi and H. E. Stanley, *Fractal Concepts in Surface Growth* (Cambridge University Press, Cambridge, England, 1995).

[8] M. Prähofer and H. Spohn, "Universal distributions for growth processes in $1+1$ dimensions and random matrices," Phys. Rev. Lett. **84**, 4882 (2000).

[9] K. Johansson, "Shape fluctuations and random matrices," Commun. Math. Phys. **209**, 437 (2000).

[10] T. Sasamoto and H. Spohn, "One-dimensional Kardar-Parisi-Zhang equation: An exact solution and its universality," Phys. Rev. Lett. **104**, 230602 (2010).

[11] K. A. Takeuchi and M. Sano, "Universal fluctuations of growing interfaces: Evidence in turbulent liquid crystals," Phys. Rev. Lett. **104**, 230601 (2010).

[12] P. Calabrese and P. Le Doussal, "Exact solution for the Kardar-Parisi-Zhang equation with flat initial conditions," Phys. Rev. Lett. **106**, 250603 (2011).

[13] T. J. Oliveira, S. C. Ferreira, and S. G. Alves, "Universal fluctuations in Kardar-Parisi-Zhang growth on one-dimensional flat substrates," Phys. Rev. E **85**, 010601 (2012).

[14] K. A. Takeuchi, M. Sano, T. Sasamoto, and H. Spohn, "Growing interfaces uncover universal fluctuations behind scale invariance," Sci. Rep. **1**, 34 (2011).

[15] C. Tracy and H. Widom, "Level-spacing distributions and the Airy kernel," Commun. Math. Phys. **159**, 151 (1994).

[16] T. Halpin-Healy, "(2+1)-dimensional directed polymer in a random medium: Scaling phenomena and universal distributions," Phys. Rev. Lett. **109**, 170602 (2012).

[17] T. J. Oliveira, S. G. Alves, and S. C. Ferreira, "Kardar-Parisi-Zhang universality class in (2+1) dimensions: Universal geometry-dependent distributions and finite-time corrections," Phys. Rev. E **87**, 040102 (2013).

[18] T. Halpin-Healy, "Extremal paths, the stochastic heat equation, and the three-dimensional Kardar-Parisi-Zhang universality class," Phys. Rev. E **88**, 042118 (2013).

[19] S. G. Alves and S. C. Ferreira, "Eden clusters in three dimensions and the Kardar-Parisi-Zhang universality class," J. Stat. Mech. **2012**, P10011 (2012).

[20] I. S. S. Carrasco and T. J. Oliveira, "Universality and geometry dependence in the class of the nonlinear molecular beam epitaxy equation," (2016), arXiv:1606.06097.

[21] J. Evans, P. Thiel, and M. C. Bartelt, "Morphological evolution during epitaxial thin film growth: Formation of 2D islands and 3D mounds," Surf. Sci. Rep. **61**, 1 (2006).

[22] T. Michely and J. Krug, *Islands, Mounds and Atoms* (Springer, Berlin, 2004).

[23] P. Meakin, *Fractals, scaling and growth far from equilibrium* (Cambridge university press, Cambridge, 1998).

[24] J. Krim and G. Palasantzas, "Experimental observations of self-affine scaling and kinetic roughening at sub-micron lengthscales," Int. J. Modern Phys. B **09**, 599 (1995).

[25] G. Palasantzas, D. Tsamouras, and J. D. Hosson, "Roughening aspects of room temperature vapor deposited oligomer thin films onto Si substrates," Surf. Sci. **507**, 357 (2002).

[26] F. Ojeda, R. Cuerno, R. Salvarezza, and L. Vázquez, "Dynamics of rough interfaces in chemical vapor deposition: Experiments and a model for silica films," Phys. Rev. Lett. **84**, 3125 (2000).

[27] J. Kelling and G. Ódor, "Extremely large-scale simulation of a Kardar-Parisi-Zhang model using graphics cards," Phys. Rev. E **84**, 061150 (2011).

[28] T. Halpin-Healy and G. Palasantzas, "Universal correlators and distributions as experimental signatures of (2+1)-dimensional Kardar-Parisi-Zhang growth," Europhys. Lett. **105**, 50001 (2014).

[29] R. A. L. Almeida, S. O. Ferreira, T. J. Oliveira, and F. D. A. A. Reis, "Universal fluctuations in the growth

of semiconductor thin films," Phys. Rev. B **89**, 045309 (2014).
[30] R. A. L. Almeida, S. O. Ferreira, I. R. B. Ribeiro, and T. J. Oliveira, "Temperature effect on $(2+1)$ experimental Kardar-Parisi-Zhang growth," Europhys. Lett. **109**, 46003 (2015).
[31] Z. Rácz and M. Plischke, "Width distribution for (2+1)-dimensional growth and deposition processes," Phys. Rev. E **50**, 3530 (1994).
[32] S. Raychaudhuri, M. Cranston, C. Przybyla, and Y. Shapir, "Maximal height scaling of kinetically growing surfaces," Phys. Rev. Lett. **87**, 136101 (2001).
[33] S. N. Majumdar and A. Comtet, "Exact maximal height distribution of fluctuating interfaces," Phys. Rev. Lett. **92**, 225501 (2004).
[34] F. Lechenault, G. Pallares, M. George, C. Rountree, E. Bouchaud, and M. Ciccotti, "Effects of finite probe size on self-affine roughness measurements," Phys. Rev. Lett. **104**, 025502 (2010).
[35] J. Villarrubia, "Morphological estimation of tip geometry for scanned probe microscopy," Surface Science **321**, 287 (1994).
[36] D. E. Wolf and J. Villain, "Growth with surface diffusion," Europhys. Lett. **13**, 389 (1990).
[37] S. Das Sarma and P. Tamborenea, "A new universality class for kinetic growth: One-dimensional molecular-beam epitaxy," Phys. Rev. Lett. **66**, 325 (1991).
[38] P. P. Chatraphorn, Z. Toroczkai, and S. Das Sarma, "Epitaxial mounding in limited-mobility models of surface growth," Phys. Rev. B **64**, 205407 (2001).
[39] S. G. Alves, T. J. Oliveira, and S. C. Ferreira, "Universal fluctuations in radial growth models belonging to the KPZ universality class," Europhys. Lett. **96**, 48003 (2011).
[40] J. M. Kim and J. M. Kosterlitz, "Growth in a restricted solid-on-solid model," Phys. Rev. Lett. **62**, 2289 (1989).
[41] S. G. Alves, T. J. Oliveira, and S. C. Ferreira, "Universality of fluctuations in the Kardar-Parisi-Zhang class in high dimensions and its upper critical dimension," Phys. Rev. E **90**, 020103 (2014).
[42] P. J. Yunker, M. A. Lohr, T. Still, A. Borodin, D. J. Durian, and A. G. Yodh, "Effects of particle shape on growth dynamics at edges of evaporating drops of colloidal suspensions," Phys. Rev. Lett. **110**, 035501 (2013).
[43] C. P. de Castro, T. A. de Assis, C. M. C. de Castilho, and R. F. S. Andrade, "Height distribution of equipotential lines in a region confined by a rough conducting boundary," J. Phys.: Cond. Matter **26**, 445007 (2014).
[44] I. S. S. Carrasco and T. J. Oliveira, "Width and extremal height distributions of fluctuating interfaces with window boundary conditions," Phys. Rev. E **93**, 012801 (2016).
[45] Rambeau, J. and Schehr, G., "Extremal statistics of curved growing interfaces in 1+1 dimensions," Europhys. lett. **91**, 60006 (2010).
[46] T. Halpin-Healy and K. A. Takeuchi, "A KPZ cocktail-shaken, not stirred..." J. Stat. Phys. **160**, 794 (2015).
[47] F. D. A. A. Reis, "Scaling of local roughness distributions," J. Stat. Mech. **2015**, P11020 (2015).
[48] K. Takeuchi and M. Sano, "Evidence for geometry-dependent universal fluctuations of the Kardar-Parisi-Zhang interfaces in liquid-crystal turbulence," J. Stat. Phys. **147**, 853 (2012).
[49] S. G. Alves, T. J. Oliveira, and S. C. Ferreira, "Non-universal parameters, corrections and universality in Kardar-Parisi-Zhang growth," J. Stat. Mech.: Theor. Exp. **2013**, P05007 (2013).
[50] S. G. Alves and J. G. Moreira, "Transitions in a probabilistic interface growth model," J. Stat. Mech. **2011**, P04022 (2011).
[51] F. F. Leal, T. J. Oliveira, and S. C. Ferreira, "Kinetic modelling of epitaxial film growth with up-and downward step barriers," J. Stat. Mech. **2011**, P09018 (2011).
[52] S. Zorba, Y. Shapir, and Y. Gao, "Fractal-mound growth of pentacene thin films," Phys. Rev. B **74**, 245410 (2006).
[53] G. Hlawacek, P. Puschnig, P. Frank, A. Winkler, C. Ambrosch-Draxl, and C. Teichert, "Characterization of step-edge barriers in organic thin-film growth," Science **321**, 108 (2008).
[54] F. Family, "Scaling of rough surfaces: effects of surface diffusion," J. Phys. A: Math.Gen. **19**, L441 (1986).
[55] F. Sagués, M. Q. López-Salvans, and J. Claret, "Growth and forms in quasi-two-dimensional electrocrystallization," Phys. Rep. **337**, 97 (2000).
[56] M. Lafouresse, P. Heard, and W. Schwarzacher, "Anomalous scaling for thick electrodeposited films," Phys. Rev. Lett. **98**, 236101 (2007).
[57] P. Córdoba-Torres, T. J. Mesquita, I. N. Bastos, and R. P. Nogueira, "Complex dynamics during metal dissolution: From intrinsic to faceted anomalous scaling," Phys. Rev. Lett. **102**, 055504 (2009).
[58] J. Felix, L. Figueiredo, J. Mendes, P. Morais, and C. de. Araujo, "Low-field microwave absorption and magnetoresistance in iron nanostructures grown by electrodeposition on n-type lightly doped silicon substrates," J. Magn. Magn. Mater. **395**, 130 (2015).
[59] J. I. Guzmán-Castañeda, A. Garcíca-Bórquez, and R. D. Arizabalo-Salas, "Fractal dimension determined through optical and scanning electron microscopy on fecral alloy after polishing, erosion, and oxidizing processes," Physica Status Solidi (b) **249**, 1224 (2012).
[60] G. Ódor, J. Kelling, and S. Gemming, "Aging of the (2+1)-dimensional Kardar-Parisi-Zhang model," Phys. Rev. E **89**, 032146 (2014).
[61] I. S. S. Carrasco, K. A. Takeuchi, S. C. Ferreira, and T. J. Oliveira, "Interface fluctuations for deposition on enlarging flat substrates," New J. Phys. **16**, 123057 (2014).
[62] J. Krug and P. Meakin, "Universal finite-size effects in the rate of growth processes," J. Phys. A: Math. Gen. **23**, L987 (1990).
[63] K. A. Takeuchi, "Experimental approaches to universal out-of-equilibrium scaling laws: turbulent liquid crystal and other developments," J. Stat. Mech. **2014**, P01006 (2014).
[64] S. G. Alves, T. J. Oliveira, and S. C. Ferreira, "Origins of scaling corrections in ballistic growth models," Phys. Rev. E **90**, 052405 (2014).
[65] S. G. Alves and S. C. Ferreira, "Scaling, cumulant ratios, and height distribution of ballistic deposition in $3+1$ and $4+1$ dimensions," Phys. Rev. E **93**, 052131 (2016).